Toward a Prediction of the Redox Properties of Electroactive SAMs: A Free Energy Calculation by Molecular Simulation

Gaëlle Filippini, Florent Goujon, Christine Bonal, and Patrice Malfreyt*

Clermont Université, Université Blaise Pascal, Laboratoire de Thermodynamique et Interactions Moléculaires, UMR CNRS 6272, BP 10448, F-63000 Clermont-Ferrand, France

We report free energy calculations of FcC_6S-/C_4S-Au and FcC_6S-/$C_{12}S$-Au binary self-assembled monolayers (SAMs) formed by one ferrocenylhexanethiolate chain and alkylthiolate chains. We demonstrate that the free energy perturbation methods are able to reproduce the positive shift of the redox potential when the coadsorbed butanethiolate C_4S chains are replaced by dodecanethiolate $C_{12}S$ chains. The different contributions to the Ewald summation involved in the perturbation process are thoroughly described. We complete the study by a microscopic description of the binary SAMs before and after oxidation. The molecular dynamics (MD) simulations evidence that the formation of the ion-pair between the ferricinium and a single perchlorate anion of the supporting electrolyte is more favored in FcC_6S-/$C_{12}S$-Au SAM.

Introduction

Self-assembled monolayers (SAMs) are well-organized arrays of organic molecules that form spontaneously from the adsorption of molecular constituents on a suitable substrate. These systems have received considerable attention recently because of their numerous applications in chemical, optical, electronic, microfabrication, and biological fields.[1–10] Among multiple-component SAM systems, electroactive monolayers comprising ferrocene-terminated thiols are probably the most widely employed and best characterized of all mixed monolayers to date.[11–18] This system has the advantage of having relatively straightforward electrochemistry in the sense that the Fe^{3+}/Fe^{2+} couple is highly reversible.

One aspect of the mixed electroactive monolayer that has been extensively investigated is the dependence of the formal potential of the surface-confined redox center on the interfacial microstructure and microenvironment of the adsorbed redox species. Thus, several studies focus on the structure–property relationships of these systems including the effects of the nature of the terminal group of the relative concentration of each component in the coating solution and of the relative chain length of the two constituents linked to the surface.[11,12,14,16,19–21]

MD simulations have shown to be highly successful in capturing both the structural and energetical properties of SAMs.[22–25] In previous molecular dynamics simulations,[23] we were first interested in developing a methodology for the molecular simulation of systems with a finite length in the third dimension.[23,24] We have applied this methodology to investigate the possible "spatial inhomogeneity" of the neutral ferrocene moieties (Fc) in $FcC_{12}S$-/$C_{10}S$-Au as a function of the surface coverage. Five reference systems were simulated using different grafting densities for ferrocenylalkylthiolates. These systems were designed to model dilute or clusterized Fc systems to study the structuring of the Fc moieties. The understanding of the ordering tendency of chains was improved by the computed quantities (density profiles, angular distributions, positions of atoms, and energetic description). The next step toward a better

understanding of these electrochemical systems was to carry out molecular dynamics simulations of the same systems in conditions close to the electrochemical experiments.[25] For this purpose, a supporting electrolyte was added ($NaClO_4$ 1M) and the redox process was modeled through structural properties of ferrocene both in its neutral (initial state) and oxidized form (final state). Then, the possibility of redox-induced orientation change was explored.

Cyclic voltammetry is extensively used to obtain the electrochemical signature of tethered ferrocenes in binary SAMs and especially to allow the determination of the redox potential $E^{\circ\prime}$. We plan to push the abilities of MD simulations in hopes to not only describe these systems, but also to obtain quantitative informations to firmly establish connections between the electrochemical experiments and MD simulations. To do so, we propose here to use the perturbation methods[26–31] over equilibrium configurations resulting from molecular dynamics simulations. We report the calculation of the difference in free energy of the redox process occurring at the electroactive label when the environment of the adsorbed redox species is changed.

Rowe and Creager[16] have demonstrated that as the alkanethiol coadsorbate chain length increases the wave corresponding to ferrocene oxidation and reduction broadens and $E^{\circ\prime}$ shifts to more positive potentials. A monolayer containing ferrocenylhexanethiol and coadsorbed dodecanethiol exhibits a formal potential almost 200 mV more positive than one containing coadsorbed butanethiol. An explanation for this positive shift arises for the fact that the redox center is partially immersed in the hydrocarbon layer and that this environment would stabilize ferrocene to a greater extent than it would for ferricinium. Two systems are then investigated here: a binary SAM formed by ferrocenylhexanethiol and coadsorbed dodecanethiol (FcC_6S-/$C_{12}S$-Au) and another binary SAM composed of ferrocenyl-hexanethiol and coadsorbed butanethiol (FcC_6S-/C_4S-Au). The fact that the electrochemical signatures of these two systems[16] are available offers direct comparison with our own calculations. Additionally, these SAMs should allow the observation of significant differences between the Gibbs free energy of redox reaction[16] ($\Delta\Delta G_{redox}^{exp} = -19.0$ kJ mol^{-1} corresponding to a shift of the redox potential of almost 200 mV).

* To whom correspondence should be addressed: E-mail: Patrice.Malfreyt@univ-bpclermont.fr.

This work is original and challenging since the calculation of thermodynamic redox properties from perturbation methods was never applied to SAMs. Actually, the traditional free energy perturbation (FEP)[26,28] and thermodynamic integration (TI)[27–29] methods are two of the most common used. These free energy calculation techniques have been successfully applied to the calculations of solubilities,[32] partition coefficients,[33] binding affinities in host−guest systems[30,34–36] and free energies of solvation[37–39] and change in redox potential for homogeneous systems.[40] However, this kind of calculation cannot be considered as systematic and routine job, especially when the perturbation between the initial and final states involves changes in the electrostatic interactions in heterogeneous environment. As a result, we take the route of accurately describing and calculating the different electrostatic energy contributions involved in the perturbation process.

The theoretical prediction of the standard redox potential in solution can be carried by several protocols.[41–43] Density functional calculations have been performed to calculate the oxidation potential for ferrocene and the redox potential of transition metal complexes.[41] Recently, a more sophisticated approach[44] combining quantum mechanical and molecular mechanical (QM/MM) methods was successfully applied to calculate the redox potentials of two hydrated flavin derivatives. Because of the large number of atoms required for simulating a binary SAM system in water, we decide to model the interactions by the use of a classical force field. As a consequence, we only focus on the calculation of redox potential shifts in SAMs.

The outline of this work is as follows. In the section concerning the simulation details, we describe the potential models and the different energy contributions for the calculation of the electrostatics. We complete this section by a short presentation of the free energy calculation. In the next section, we present the results through a methodological section and compare the simulated redox properties with experiments. We then give a microscopic description associated with an energy characterization of these SAMs in the oxidized and reduced states. We conclude this paper by a summary of the main results.

Simulation Details

Interaction Model. The system consists of five layers of a Au(111) surface grafted with either n-C_4 alkylthiol (C_4H_9S) or n-C_{12} alkylthiol ($C_{12}H_{25}S$) molecules and one FcC$_6$S ferrocenylhexanethiol ($C_{16}H_{21}FeS$). We used the all-atom (AA) version of the Cornell force field AMBER[45] for grafted molecules. The Au parameters were taken from the work of Ayappa and co-workers.[46] The ferrocene part was modeled using the parameters described by Canongia et al.[47] The general potential function is of the form

$$U = U_{bond} + U_{angle} + U_{dihedral} + U_{LJ} + U_{ele} \quad (1)$$

where

$$U_{bond} = \sum_{bonds} \frac{1}{2}k_b(r - r_o)^2 \quad (2)$$

$$U_{angle} = \sum_{angles} \frac{1}{2}k_\theta(\theta - \theta_o)^2 \quad (3)$$

$$U_{dihedral} = \sum_{dihedrals} k_\phi[1 + \cos(l\phi + \delta)] \quad (4)$$

$$U_{LJ} = \sum_{i=1}^{N-1} \sum_{j>i}^{N} 4\varepsilon_{ij}\left[\left(\frac{\sigma_{ij}}{r_{ij}}\right)^{12} - \left(\frac{\sigma_{ij}}{r_{ij}}\right)^{6}\right] \quad (5)$$

where k_b, k_θ, and k_ϕ are the force constants for deformation of bonds, angles, and dihedrals, respectively. The equilibrium values of bond distances and valence angles correspond to r_o and θ_o, respectively. In the dihedral angle term, l is the periodicity and δ is the phase factor. The C−H covalent bonds were kept of fixed length by using the SHAKE algorithm.[48] The intermolecular and intramolecular interactions due to the repulsion−dispersion interactions are calculated using the Lennard-Jones (LJ) potential, represented by eq 5. In the AMBER force field, the nonbonded interactions between atoms separated by exactly three bonds (1−4 LJ interactions) are reduced by a factor of 0.5.[45] The Lennard-Jones potential parameters for the interactions between unlike atoms were calculated by using the Lorentz−Berthelot mixing rules (quadratic and arithmetic rules for ε_{ij} and σ_{ij} parameters, respectively). The water molecules were represented by the TIP4P/2005 model.[49] As the system is nonperiodic in the direction normal to the surface (z-axis), the simulation cell is closed by an additional gold layer. The distance between the two inner surfaces was chosen to be 50 Å, which is large enough for the water molecules in the middle of the cell to have a bulk behavior.[50] A supporting electrolyte NaClO$_4$ is added in the water phase. The ClO$_4^-$ ions are represented using the model described by Wu et al.[51] A typical configuration of the system with C$_4$S coadsorbed chains is shown in Figure 1a. The density profiles of some species are also given in Figure 1b along the normal to the surface to allow a better representation of the local distribution of each constituent of the SAM.

Electrostatic Interactions. In addition to the LJ interactions, the electrostatic interactions are calculated with the full Ewald summation technique.[52,53] For a neutral periodic system with orthogonal axis, the electrostatic potential U_{ele} is defined as

$$U_{ele} = U_R + U_K + U_{self} + U_{excl} + U_{M_z} \quad (6)$$

The real space part U_R of the potential is given by

$$U_R = \frac{1}{8\pi\varepsilon_o} \sum_i \sum_a \sum_{j\neq i} \sum_b q_{ia}q_{jb}\frac{\text{erfc}(\alpha r_{iajb})}{r_{iajb}} \quad (7)$$

where the sums are over all atoms a in molecule i and all atoms b in molecule j. r_{iajb} is the distance between the atoms a and b belonging to two different molecules i and j and q_{ia} and q_{jb} represent the charges on atoms a and b, respectively. This term is pairwise-additive and short-ranged and a spherical cutoff can be used with periodic boundary conditions. α is chosen so that only atom−atom pair interactions between different molecules in the central cell ($n = 0$) need to be considered. erf(x) is the error function whereas erfc(x) is the complementary error function. Note that the overall charge of the simulation box must be zero.
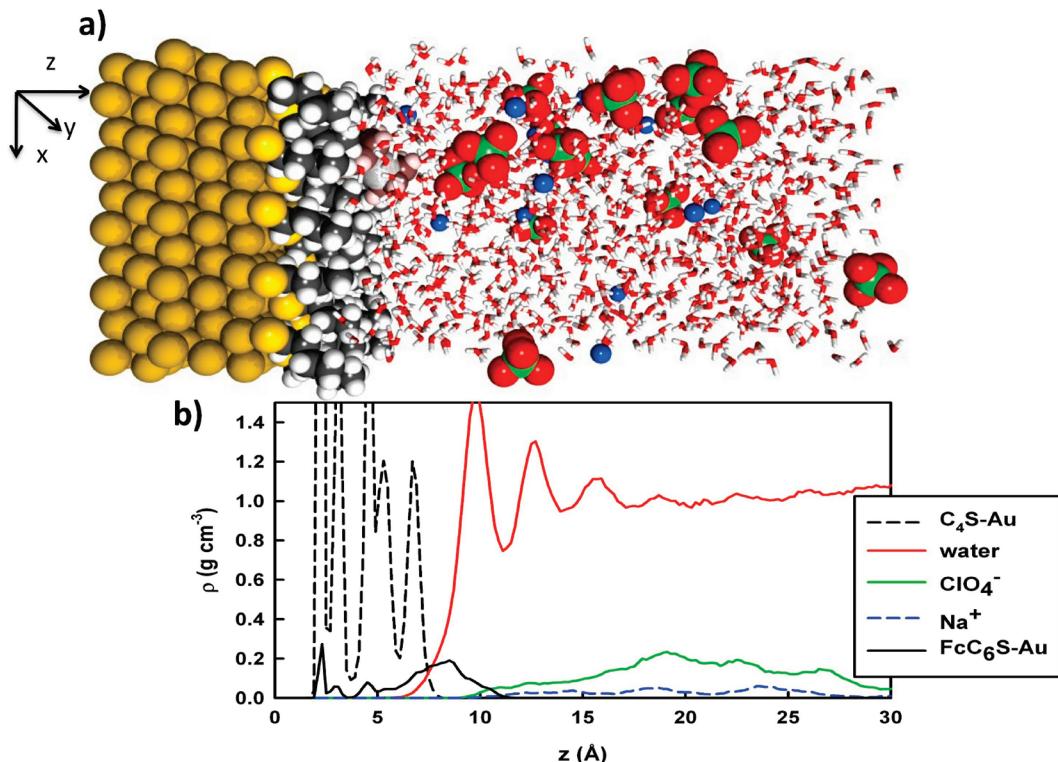
Prediction of Redox Properties of Electroactive SAMs

J. Phys. Chem. B, Vol. 114, No. 40, 2010 **12899**

Figure 1. (a) Typical configuration of the simulation cell of the FcC$_6$S-/C$_4$S-Au SAM. (b) We give for completeness the molecular density profiles of the ferrocenylhexanethiolate chain (FcC$_6$S-Au), coadsorbed butanethiolate chains (C$_4$S-Au), water, Na$^+$, and ClO$_4^-$ counterions.

The reciprocal space part U_K of the potential is expressed as

$$U_K = \frac{1}{2V\varepsilon_o} \sum_{k \neq 0} \frac{1}{k^2} \exp\left(-\frac{k^2}{4\alpha^2}\right) \left| \sum_i \sum_a q_{ia} \exp(i\mathbf{k} \cdot \mathbf{r}_{ia}) \right|^2 \tag{8}$$

where V is the simulation cell volume, r_{ia} is the Cartesian coordinate of site a in molecule i. The reciprocal lattice vector $\mathbf{k}$ is defined as $\mathbf{k} = 2\pi(l/L_x\mathbf{u}, m/L_y\mathbf{v}, n/L_z\mathbf{w})$ where $\mathbf{u}$, $\mathbf{v}$, and $\mathbf{w}$ are the reciprocal space basis vectors and l, m, n take values of $0, \pm 1, \pm 2, ..., \pm\infty$. The reciprocal space sum is truncated at an ellipsoidal boundary at the vector $|\mathbf{k}^{max}|$. This term includes all the intramolecular interactions due to the bonded atoms.

The U_{excl} term is added to correct for the contributions due to intramolecular electrostatic interactions. It is expressed as

$$U_{excl} = -\frac{1}{8\pi\varepsilon_o} \sum_i \sum_a \sum_{b \neq a} q_{ia}q_{ib} \frac{\text{erf}(\alpha r_{iaib})}{r_{iaib}} \tag{9}$$

where the sums are over atoms bonded to atoms a and b of the same molecule i through bonds, valence, and dihedral potentials.

A fourth correction U_{self} term is required to correct for the fact that the sum of Gaussian functions in the real space includes the interactions of each Gaussian with itself

$$U_{self} = -\frac{\alpha}{4\pi^{3/2}\varepsilon_o} \sum_i \sum_a q_{ia}^2 \tag{10}$$

A fifth term, U_{M_z}, is included to consider the supercell approximation[54] and is defined as

$$U_{M_z} = \frac{1}{2\varepsilon_o V} M_z^2 \tag{11}$$

where M_z is the net dipole moment of the simulation cell given by $\sum_{i=1}^{N} q_i\mathbf{r}_i$. This contribution is the correction term of Yeh and Berkowitz[54] which results from the plane-wise summation method proposed by Smith.[53] Adding this term to the total energy implies the use of a z-component force for each atom given by

$$F_{i,z} = -\frac{q_i}{\varepsilon_o V} M_z \tag{12}$$

The supercell approximation[54] consists of elongating the z-dimension of the simulation cell by placing an empty space of at least four times the space of the fluid-occupied region. The use of this approximation and the dipole correction allows one to apply the conventional three-dimensional Ewald summation technique to the calculation of the electrostatic interactions in a slab geometry.[50]

Free Energy Calculations. The difference in Helmholtz free energies ΔA between molecular systems (0) and (1) can be calculated with the free energy perturbation (FEP)[26,28] and thermodynamic integration (TI)[26–31] methods. In the FEP approach, the computation of the free energy difference between two states (0) and (1) in the constant-NVT ensemble is split into N_w intermediate contiguous states or windows defined by a coupling constant λ

$$\Delta A_{FEP} = A_1 - A_0 = \sum_{i=1}^{N_w} \Delta A(\lambda_i) =$$

$$\sum_{\lambda=0}^{1} - RT \ln\left\langle \exp\left[-\frac{(U(r, \lambda \pm \Delta\lambda) - U(r,\lambda))}{RT}\right]\right\rangle_{\lambda} \quad (13)$$

where $U(r, \lambda)$ is the potential energy corresponding to state λ and depending only on the atomic coordinate set $\mathbf{r}$. R is the molar gas constant, T is the absolute temperature and $\langle \ \rangle$ denotes a canonical ensemble average reflecting state λ.

The TI method expresses the change in free energy as the following integral

$$\Delta A_{TI} = \int_0^1 \left\langle \frac{\partial U(r,\lambda)}{\partial \lambda}\right\rangle_{\lambda} d\lambda \quad (14)$$

The derivative of $U(r, \lambda)$ with respect to λ can be calculated using a central finite difference technique between $U(r, \lambda + \delta\lambda)$ and $U(r, \lambda - \delta\lambda)$

$$\left\langle \frac{\partial U(r,\lambda)}{\partial \lambda}\right\rangle_{\lambda,CD} = \left\langle \frac{U(r, \lambda + \delta\lambda) - U(r, \lambda - \delta\lambda)}{2\delta\lambda}\right\rangle_{\lambda} \quad (15)$$

The perturbations are performed in both directions ("double-wide sampling") with N_w windows over the entire simulation. The derivative can be calculated in the forward $(+\delta\lambda)$ direction using the following expression

$$\left\langle \frac{\partial U(r,\lambda)}{\partial \lambda}\right\rangle_{\lambda,F} = \left\langle \frac{U(r, \lambda + \delta\lambda) - U(r, \lambda)}{\delta\lambda}\right\rangle_{\lambda} \quad (16)$$

whereas the same derivative can be calculated in the backward direction by replacing $U(r, \lambda + \delta\lambda)$ by $U(r, \lambda - \delta\lambda)$.

The finite difference integration thermodynamic (FDTI) method uses the perturbation formalism to calculate the derivative of the Hamiltonian with respect to λ as

$$\left\langle \frac{\partial U(r,\lambda)}{\partial \lambda}\right\rangle_{\lambda,CD} = \frac{\partial A(\lambda)}{\partial \lambda} \simeq \frac{\Delta A(\lambda)}{\delta \lambda} = $$
$$ - \frac{RT}{2\delta\lambda} \ln\left\langle \exp\left[-\frac{(U(r, \lambda + \delta\lambda) - U(r, \lambda - \delta\lambda))}{RT}\right]\right\rangle \quad (17)$$

The change in the Helmholtz free energy ΔA_{FDTI} is thus expressed as the integral of $\langle [\partial U(r, \lambda)]/(\partial \lambda)\rangle_{\lambda}$ calculated using eq 17. $\delta\lambda$ is taken sufficiently small $(\delta\lambda = 0.0001)$ to avoid hysteresis between calculations carried out from state λ to state $\lambda + \delta\lambda$ and from state λ to state $\lambda - \delta\lambda$.

Simulations in the forward $(+\delta\lambda)$ and backward $(-\delta\lambda)$ directions give an estimate of the statistical uncertainty for the TI and FDTI approaches. The integration over λ for both techniques is carried out by a trapezoidal algorithm and also by fitting the integrand as a function of λ and integrating it analytically.

Computational Procedures

Simulation Cell. The gold surface was composed by five (111) layers of a 9×10 FCC lattice, so that the dimensions of the simulation box along x and y axis were 25.9 and 24.9 Å, respectively. One ferrocenyhexanethiolate (FcC_6S) chain was grafted onto the surface with an initial tilt angle $\theta = 30°$. The remaining space was filled by grafting either 27 C_4S or 27 $C_{12}S$ alkylthiolate chains, using a minimal distance between grafting points corresponding to the experimental surface coverage of 1/3. This results in a ferrocene surface coverage of 2.5×10^{-11} mol cm^{-2} (5% of a full monolayer) in line with the corresponding experimental coverage.[16] The simulation cell was closed by an additional gold layer formed by 90 gold atoms. The separation distance between the two surfaces was fixed to 50 Å. The simulation cell was then elongated in the z-direction to yield a L_z dimension of 300 Å.

Two systems A and B were considered. The system A corresponding to the FcC_6S-/C_4S-Au SAM was formed by one grafted ferrocenylalkylthiolate chain and 27 grafted n-butanethiolate (C_4S) chains, 900 water molecules, 16 sodium cations, and 16 perchlorate anions. The system B corresponding to the FcC_6S-/$C_{12}S$-Au SAM was formed by one grafted ferrocenylalkylthiolate chain and 27 grafted n-dodecanethiolate ($C_{12}S$) chains, 668 water molecules, 12 sodium cations, and 12 perchlorate anions. The water, Na^+ and ClO_4^- molecules were randomly added in the remaining volume to respect a concentration of 1 M for the supporting electrolyte and an accurate bulk density for water. This value of concentration is in line with the experimental conditions.[16]

Simulations were run in the constant-NVT statistical ensemble using Nose-Hoover thermostat[55] with a coupling constant of 0.5 ps. The equations of motion were integrated using the Verlet leapfrog algorithm scheme at $T = 298$ K with a time step equal to 2 fs. The cutoff radius for the Lennard-Jones and the real space of the electrostatic interactions was fixed to 12 Å. We also used a reciprocal space cutoff radius of 1.14 $Å^{-1}$. The convergence parameter α was fixed to 0.2651 $Å^{-1}$. The maximum reciprocal lattice vectors parallel to the gold surfaces were given by $k_x^{max} = k_y^{max} = 7$. As the simulation cell was elongated along z, k_z^{max} was increased up to 80. This price must be paid to use the standard three-dimensional Ewald summation in a slab geometry and to account for the long-range electrostatic interactions accurately. With these parameters, the calculation of the electrostatic interactions using the Ewald summation yields a relative error of 10^{-6}. The configurations were generated using the parallel version of the modified DL_POLY_MD package[56] by using up to 8 processors at a time. A typical NVT simulation run consists of an equilibrium period of 500 ps and an additional production phase of 400 ps.

Perturbation Process. The oxidation of the ferrocene moiety in the ferrocenylalkylthiolate chain in the A and B systems is carried out by using a perturbation process. It consists in changing the charge of the ferrocene moiety from 0.0 ($\lambda = 0.0$) to 1.0 ($\lambda = 1.0$). The partial charges of the ferrocene group are taken from the force field developed by Canongia et al.[47] The partial charges of the ferricinium group have been calculated from the density functional theory (DFT)[57,58] (B3LYP)[59-61] with effective core potential (SD-DALL) Gaussian basis using the Gaussian 03 package[62] and the CHELPG[63] procedure as a grid-based method. The perturbation of the partial charges affects all the atoms of the ferrocene group and the last three methylene groups of the alkyl chain bounded to ferrocene through bonds, valence, and dihedral angle potentials as illustrated in Figure 2. To respect the electroneutrality in the system, a sodium cation vanishes between $\lambda = 0.0$ and $\lambda = 1.0$. The perturbation is carried over 11 contiguous states or windows defined by the coupling parameter λ. The variations of the potential energy $U(r, \lambda)$ during the mutation of the sodium cation are calculated using a linear combination of the LJ parameters (σ, ϵ) of the
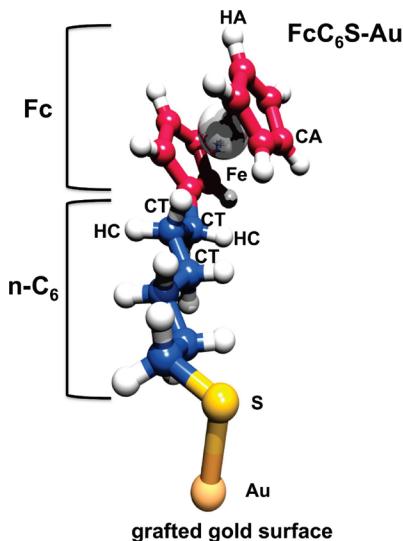
Prediction of Redox Properties of Electroactive SAMs

J. Phys. Chem. B, Vol. 114, No. 40, 2010 **12901**

Figure 2. Labeling scheme of the ferrocenylhexanethiolate chain (FcC$_6$S-Au) used in this work. The partial charges of the different atom types between the reduced and oxidized states are given in Table 1.

initial state (0) ($\lambda = 0.0$) and final state (1) ($\lambda = 1.0$) using the following mixing rules

$$\varepsilon_{ij}(\lambda) = \lambda(\sqrt{(\varepsilon_{ii}(1)\varepsilon_{jj})}) + (1 - \lambda)(\sqrt{(\varepsilon_{ii}(0)\varepsilon_{jj})}) \quad (18)$$

$$\sigma_{ij}(\lambda) = \lambda\left(\frac{\sigma_{ii}(1) + \sigma_{jj}}{2}\right) + (1 - \lambda)\left(\frac{\sigma_{ii}(0) + \sigma_{jj}}{2}\right) \quad (19)$$

where i and j represent perturbed and unperturbed atom types, respectively. The atomic site charge q is also expressed as a function of λ as follows

$$q_i(\lambda) = \lambda q_i(1) + (1 - \lambda)q_i(0) \quad (20)$$

where i represents the perturbed atomic site. The values of the partial charges for the ferrocene and methylene groups as well as the Lennard-Jones parameters for the sodium cations are given for completeness in Table 1 for the initial and final states. The total simulation for completing the perturbation calculation over 11 windows is about 10 ns.

Results and Discussions

The redox reactions represented in Scheme 1 allow us to compare the difference in the calculated Helmholtz free energies $\Delta\Delta A = \Delta A_B - \Delta A_A$ where A refers to FcC$_6$S-/C$_4$S-Au SAM and B to FcC$_6$S-/C$_{12}$S-Au SAM with the experimental results. Because the oxidative reactions are simulated here, the computed Helmholtz free energies are of opposite sign compared to experimental free energies that correspond to reductive processes. By assuming that the properties (pressure, density) of some species in our NVT simulations correspond to those that one would obtain from NpT simulations at a constant standard pressure of 1 bar, and that the pV term is constant along the path from $\lambda = 0.0$ to $\lambda = 1.0$, we may then assimilate $\Delta\Delta A$ to $-\Delta\Delta G_{\text{redox}}^{\text{cal}}$. We may also compare the calculated $\Delta\Delta G_{\text{redox}}^{\text{cal}}$ with the experimental $\Delta\Delta G_{\text{redox}}^{\text{exp}}$ property. This is verified in Figure 1b by the density of water, which is close to 1 g cm^{-3} in the bulk water region. We also check that the product pV does not

TABLE 1: Partial Charges for the Atoms of the Ferrocene Group and Methylene Groups of the Alkyl Chains, Lennard-Jones Parameters for the Sodium Cation in the Initial State ($\lambda = 0.0$) and Final State ($\lambda = 1.0$) in the A and B Systems[a]

parameters	initial state $\lambda = 0$	final state $\lambda = 1.0$
	CA	
q (e)	−0.1	−0.04433
	HA	
q (e)	0.090	0.14040
	Fe	
q (e)	0.10	0.17970
	CT	
q (e)	−0.090	−0.120
	HC	
q (e)	0.060	0.060
	Na	
q (e)	1.0	0.0
σ (Å)	2.35	0.0
ε (kJ mol^{-1})	0.5438	0.0

[a] The atom types are illustrated in Figure 2.

change within the statistical fluctuations between the initial and final states. The experimental $\Delta\Delta G_{\text{redox}}^{\text{exp}} = \Delta G_B - \Delta G_A$ redox property can be assimilated to $-nF\Delta\Delta E^{\circ\prime}$ where F is the Faraday's constant and n equals to 1. The $\Delta\Delta E^{\circ\prime}$ corresponds to the shift in redox potential when the alkanethiol coadsorbate length increases from 4 to 12. The experimental[16] $\Delta\Delta E^{\circ\prime}$ change in the redox potential is about 200 mV and corresponds to a negative contribution of about −19 kJ mol^{-1} for $\Delta\Delta G_{\text{redox}}^{\text{exp}}$.

Methodological Discussions. To have a better evaluation of the impact of the perturbation over the free energy calculation, the total ΔA property has been separated into specific ΔA_i contributions. These contributions correspond to the different parts of the energy involved in the Ewald summation method and to the species involved (ferrocene, sodium) in the perturbation process. Before a discussion of these different contributions, we represent in Figure 3a,b the trajectories of the free energy derivative for the total contribution and the real part ($U_{R,Fc}$) of the electrostatic potential at $\lambda = 0.0$ in the system B. Figure 3a,b shows that the total free energy and the contribution of the real space converge very well after 200 ps. This check allows to ascertain the accuracy of our free energy calculation for binary SAMs. The convergence of the free energy in SAMs requires simulation times much higher than those used in bulk systems.[30]

The mutations from $\lambda = 0.0$ to $\lambda = 1.0$ in systems A and B involve the oxidation of the ferrocene group and the mutation of the sodium atom to a ghost particle with no interaction with the remaining molecules in the system. The annihilation of the sodium does not aim at modeling the experimental conditions but at respecting the electroneutrality in the simulation box required by the use of the Ewald technique. However, other alternatives are possible such as either progressively negatively charging the atoms of the opposite gold layer or progressively adding one perchlorate anion in the solution. The position of the pseudosodium atom is then kept fixed during the perturbation process to avoid that the cation visits any spot in the simulation cell.

Actually, this mutation also includes a part of the Gibbs free energy of hydration (ΔG_{hyd}^o) of the sodium. The contribution of the electrostatics in the perturbation is analyzed by splitting the Helmholtz free energy into $\Delta A_{R,F_C}$, ΔA_K, ΔA_{excl}, ΔA_{self}, ΔA_{M_z}

TABLE 2: Different Helmholtz Free Energy Contributions ΔA (kJ mol^{-1}) Calculated in the Two Systems Using the TI and FDTI Approaches[a]

	(A) FcC$_6$S-/C$_4$S-Au				(B) FcC$_6$S-/C$_{12}$S-Au			
	ΔA_B	ΔA_F	ΔA_C	ΔA_{Fit}	ΔA_B	ΔA_F	ΔA_C	ΔA_{Fit}
				$\Delta A_{R, F_C}$				
TI	5.5	−5.4	−5.5	−5.9	1.1	−1.1	−1.1	−1.4
FDTI	5.5	−5.5	−5.5	−5.9	1.1	−1.1	−1.1	−1.4
				ΔA_K				
TI	−27.1	27.2	27.1	28.0	−41.4	41.5	41.5	42.8
FDTI	−27.1	27.2	27.1	28.0	−41.4	41.5	41.5	42.8
				ΔA_{excl}				
TI	−17.7	17.6	17.7	17.0	−17.7	17.7	17.7	17.1
FDTI	−17.7	17.6	17.7	17.0	−17.7	17.7	17.7	17.1
				ΔA_{self}				
TI	−194.4	194.4	194.4	194.2	−194.4	194.4	194.4	194.2
FDTI	−194.4	194.4	194.4	194.4	−194.4	194.4	194.4	194.2
				ΔA_{M_z}				
TI	0.02	−0.02	−0.02	−0.02	0.02	−0.02	−0.02	−0.02
FDTI	0.02	−0.02	−0.02	−0.02	0.02	−0.02	−0.02	−0.02
				$\Delta A_{R, Na}$				
TI	−313.9	313.9	313.9	313.6	−308.5	308.5	308.5	308.5
FDTI	−313.9	313.9	313.9	313.6	−308.6	308.5	308.5	308.4
				$\Delta A_{LJ, Na}$				
TI	161.1	−161.0	−161.0	−161.5	157.9	−157.7	−157.8	−158.3
FDTI	161.0	−161.0	−161.0	−161.5	157.8	−157.8	−157.8	−158.4

[a] ΔA_B and ΔA_F are the Helmholtz free energies calculated in the backward and forward directions, respectively. ΔA_C and ΔA_{Fit} are the free energies calculated from integrations using a trapezoidal rule and a fit procedure, respectively.

SCHEME 1: Redox Reactions Used to Model the Effect of the Environment on the Change in the Redox Properties of FcC$_6$S-/C$_4$S-Au (System A Represented by (Fc)$_A$) and FcC$_6$S-/C$_{12}$S-Au (System B Represented by (Fc)$_B$) SAMs[a]

$$(Fc^+)_A + e^- \xrightarrow{-\Delta A_A} (Fc)_A$$

$$(Fc^+)_B + e^- \xrightarrow{-\Delta A_B} (Fc)_B$$

[a] The experimental redox property $-\Delta G_{redox}^{exp} = F\Delta\Delta E^{\circ\prime}$ can be compared to $\Delta\Delta A = \Delta A_B - \Delta A_A$.

typical contributions. These contributions calculated with the TI and FDTI approaches are listed in Table 2 for the A and B systems. $\Delta A_{R, F_C}$ is a contribution calculated from the real space of the potential (eq 7) in the Ewald summation method by considering only the perturbed atoms. ΔA_K corresponds to the contributions of the reciprocal space of the electrostatic potential calculated using eq 8 over all of the atoms of the simulation cell. ΔA_{excl} corresponds to an atomic self-correction that considers the atoms interacting with the perturbed atoms through bonds, valence and dihedral angle potentials. ΔA_{self} of eq 10 considers only the perturbed atoms and ΔA_{M_z} is the contribution imposed by the use of the supercell approximation for a correct description of the electrostatic in a slab geometry. Even if some of these contributions are small or vanish between the two states, it seems very important to us, from a theoretical aspect, to estimate the magnitude of these contributions and their impact on this study. We check then that the free energy contributions ΔA_{excl}, ΔA_{self}, and ΔA_{M_z} vanish in the $\Delta\Delta A$ difference even if the magnitudes of ΔA_{excl} and ΔA_{self} are quite important.

Table 2 shows that the ΔA contributions calculated in the backward and forward directions are equal in magnitude and are in opposite sign as expected for a thermodynamic consis-

tency of a reversible path. This also means that the value of $\delta\lambda = 10^{-4}$ is appropriate for the perturbation of these systems. The convergence of the different contributions within the simulation time, the equivalence between the TI and FDTI approaches (see Table 2), the accuracy between the values calculated in the forward and reverse directions make the free energy calculation in these SAMs consistent from a methodological viewpoint. Figure 4 shows the average values of $\langle(\partial U(r, \lambda))/(\partial\lambda)\rangle_\lambda$ as a function of the coupling parameter for the sum of all the energy contributions, the real and reciprocal parts of the electrostatic potential in the A and B systems. We observe in panels a and b of Figure 4 that the evolution of the total contribution $\langle[\partial U(r, \lambda)]/(\partial\lambda)\rangle_\lambda$ with λ decreases unlinearly for the two systems. Fitting the curve represents an interesting alternative compared to the numerical trapezoidal integration since it allows to average the fluctuations close to the end point ($\lambda = 1.0$). We check that the fitted curve matches very well the values in the forward and backward directions. The values calculated using the trapezoidal rules and the fit procedure are given in Table 2 for completeness. The maximum deviation between these two integration methods is about 0.5 kJ mol^{-1}.

Some values of ΔA can reach 300 kJ mol^{-1} (see Table 2). Provided that the perturbation is carried out over 11 windows, the ΔA value calculated by FEP over one window would be about 30 kJ mol^{-1}. This order of magnitude is too large to allow for the convergence of ΔA with the FEP method. The number of windows should be increased up to 100 to obtain a convergence of ΔA and an energy difference ΔU in the order of $k_B T$ using FEP. This would make the simulation too time-consuming and explains why we only use the TI and FDTI approaches in this work.

We now focus on the annihilation of the sodium cation between $\lambda = 0.0$ and $\lambda = 1.0$. The perturbation is then decomposed into the Lennard-Jones and electrostatic contributions. These two contributions are given for each system in Table
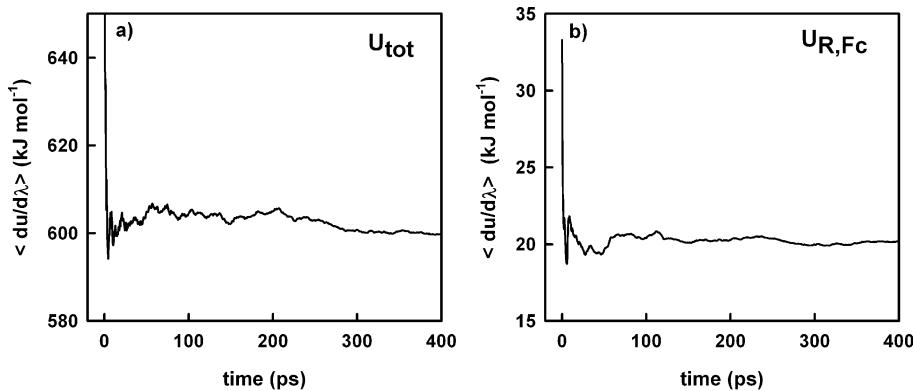
Prediction of Redox Properties of Electroactive SAMs

J. Phys. Chem. B, Vol. 114, No. 40, 2010 **12903**

Figure 3. Cumulated average value of the $\langle[(\partial U(r, \lambda)]/(\partial\lambda)\rangle_\lambda$ term as a function of time at $\lambda = 0.0$ for (a) the total contribution and (b) the real space of the potential calculated from the perturbed atoms.
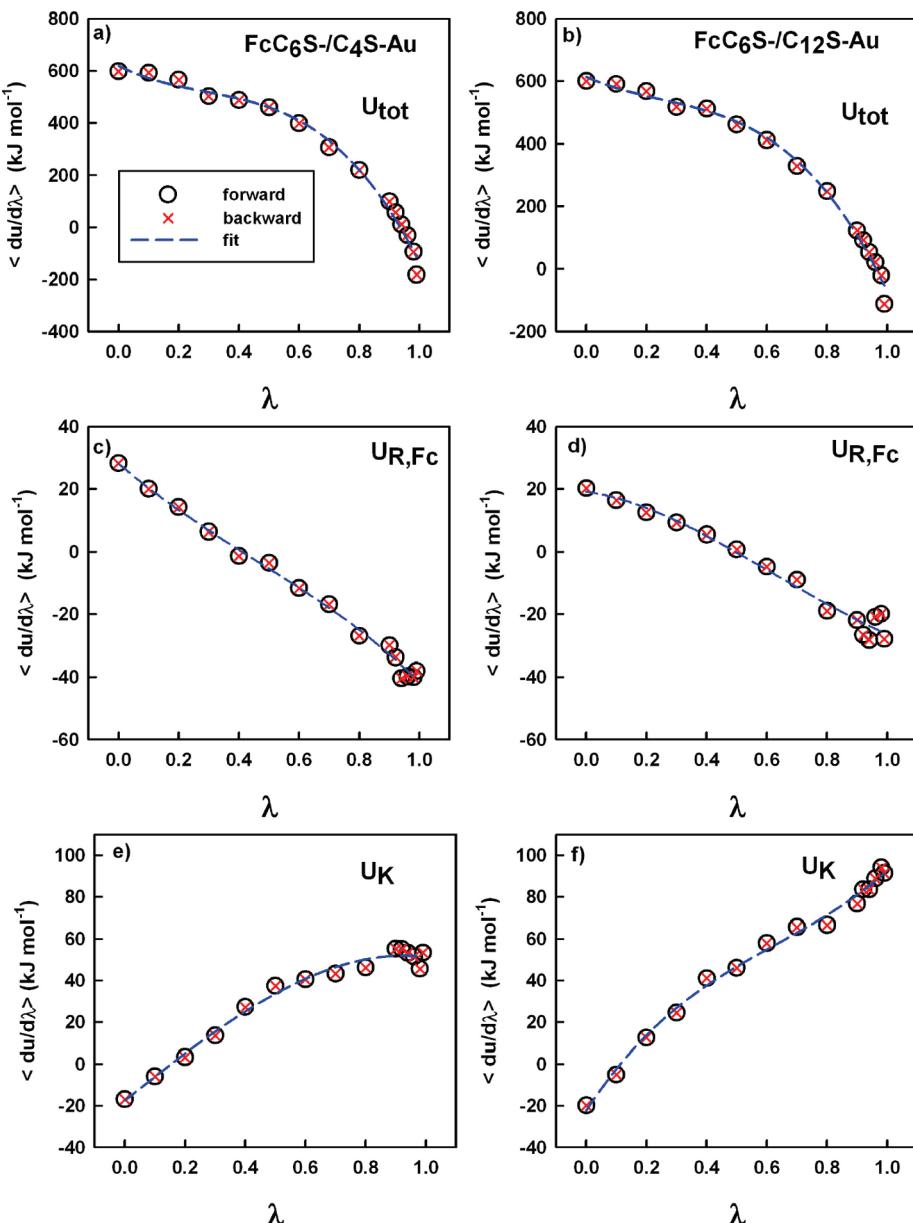

Figure 4. Average $\langle(\partial U(r, \lambda))/(\partial\lambda)\rangle_\lambda$ value as a function of λ calculated in the forward and backward directions. The dashed lines correspond to the fit of the central difference calculated from eq 15. The graphs on the left-side correspond to the FcC_6S-/C_4S-Au system whereas those on the right-side correspond to he FcC_6S-/$C_{12}S$-Au system. The different contributions are indicated for each graph and explained in the text of the paper.

2. The evolution of the derivative of the potential with respect to the coupling parameter is given in the Appendix for the two

energy contributions for each SAM. In each system, the sodium cation is constrained at a given z-position ($z = 44$ Å) close to

TABLE 3: Differences in the Helmholtz Free Energy Contributions (kJ mol^{-1}) between the A and B Systems[a]

	(A)		(B)		(B) − (A)	
	ΔA_C	ΔA_{Fit}	ΔA_C	ΔA_{Fit}	$\Delta\Delta A_C$	$\Delta\Delta A_{Fit}$
$\Delta A_{R, F_C}$	−5.5	−5.9	−1.1	−1.4	4.4	4.5
ΔA_K	27.2	28.0	41.5	42.8	14.3	14.8
ΔA_{excl}	17.7	17.0	17.7	17.1	0.0	0.1
ΔA_{self}	194.4	194.2	194.4	194.2	0.0	0.0
ΔA_{M_z}	−0.02	−0.02	−0.02	−0.02	0.0	0.0
$\Delta A_{R, Na}$	313.9	313.6	308.5	308.5	−5.4	−5.1
$\Delta A_{LJ, Na}$	−161.0	−161.5	−157.8	−158.3	3.2	3.2
$\sum_i \Delta A_i$	386.7	385.4	403.2	402.9	16.5	17.5
$-\Delta\Delta G_{redox}^{cal}$					17.0	
$-\Delta\Delta G_{redox}^{exp}$					19.0	

[a] The sum of the different free energy contributions is represented by $\sum_i \Delta A_i$. The experimental $-\Delta\Delta G_{redox}^{exp}$[16] is given for comparison. The calculated $-\Delta\Delta G_{redox}^{cal}$ is averaged over the values computed from the fit and the trapezoidal integrations.

the outermost surface. The sodium-surface separation distance is large enough to maintain the first hydration shell around the sodium. The surface affects the second hydration shell and significant differences with a sodium cation in bulk water appears from sodium−water separation distances of 5.8 Å. This means that a certain number of water molecules does not participate to the interaction with the sodium due to the presence of the surface. This explains why the ΔA contribution for the sodium is smaller than the Gibbs free energy of hydration[64] ($\Delta G_{hyd}^o = -410$ kJ mol^{-1}). We obtain a positive value for ΔA because our transformation corresponds to the annihilation of the sodium cation. ΔA is 152.1 kJ mol^{-1} for the system A and 150.2 kJ mol^{-1} for the system B. We also observe that the annihilation of the sodium cation is approximately the same in A and B. Table 3 shows a difference of about −2 kJ mol^{-1} that corresponds to the sum of $\Delta A_{R, Na}$ and $\Delta A_{LJ, Na}$ whereas no contribution is expected from the thermodynamic cycle. Actually, this contribution results from the fact that the environment of the sodium cation is not really identical in the two systems. This can be attributed to finite size effects in our simulation cells.

Comparison with Experiments and Microscopic Interpretation. We report in Table 3 the different ΔA_i contributions calculated in systems A and B as well as the difference $\Delta\Delta A_i$ calculated between B and A. The sum of the different contributions can be compared to the available thermodynamic redox property $-\Delta\Delta G_{redox}^{exp}$. We find excellent agreement between the simulated and experimental redox property. The free energy calculation is then in line with experiments to conclude that the ferrocene oxidation is thermodynamically unfavored in SAMs with coadsorbed dodecanethiol chains compared to SAMs with coadsorbed butanethiol chains. The change in the redox potential is reproduced within a deviation less than 13% from experiments. This deviation is reduced to 2% if we assume that the annihilation of the sodium cation is identical in the two systems.

To complete this study, we are interested in the microscopic description of these binary SAMs in the initial ($\lambda = 0.0$) and final ($\lambda = 1.0$) states. We begin the discussion by representing in Figure 5 the molecular density profiles of coadsorbed C_4S butanethiol chains, FcC_6S ferrocenylhexanethiol chain, water, ClO_4^-, and Na^+ counterions. The initial state with the ferrocene headgroup is represented in panel a of this figure whereas panel b shows the density profiles in the final state where the ferrocene is oxidized. Panels c and d of Figure 5 show the same profiles with coadsorbed $C_{12}S$ dodecanethiol chains. From the profiles
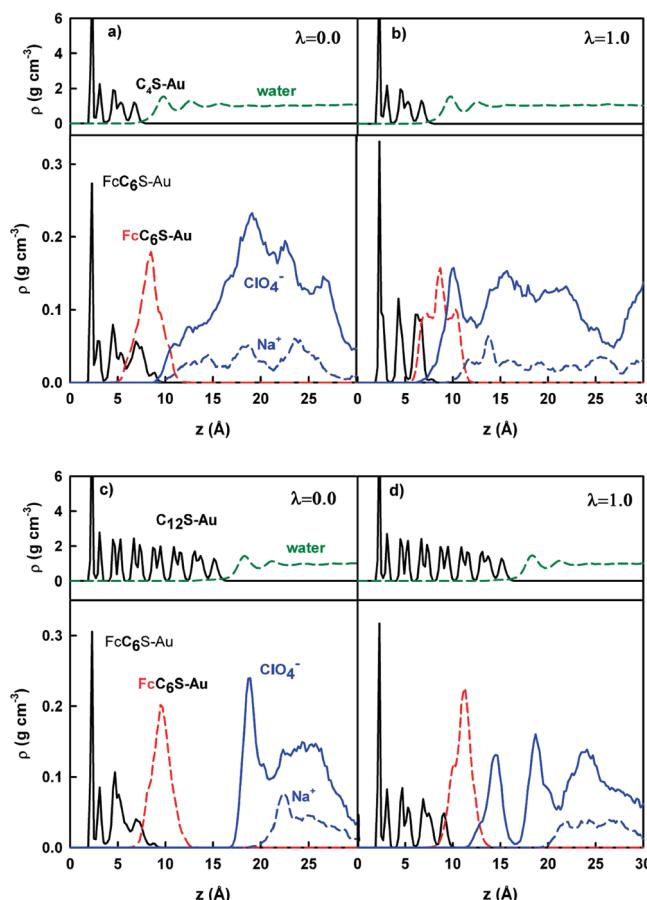

Figure 5. Molecular density profiles on the coadsorbed butanethiolate chains (C_4S-Au) chains, ferrocenylhexanethiolate chain (FcC_6S-Au), water, and counterions for (a) $\lambda = 0.0$ and (b) $\lambda = 1.0$. The same profiles are given in panels (c) and (d) where the dodecanethiolate ($C_{12}S$-Au) chains replace the coadsorbed butanethiolate (C_4S-Au) chains.

of water, we observe typical alkane−water interfaces with no water molecule within the alkane region. The position of the alkane−water interface depends on the length of the alkylthiolate chain and does impact on the solvation of the different counterions close to the end groups of the monolayer.

We now focus on the state ($\lambda = 0.0$) corresponding to the ferrocene headgroup before oxidation (Figure 5a,c). In system A, we observe a small domain where the profile of the ferrocene group overlaps the molecular density profile of its alkyl chain. This is consistent with the tilting of the terminal part of the chain due to the hydrophobic character of the ferrocene headgroup. A typical configuration of this system A is shown in panel a of Figure 6. This overlap is not observed in system B indicating that the orientation of the ferrocene is quite different. In system B, an important overlap between the density profiles of the Fc group and the diluant C_{12} chains is also highlighted. This underlines the alkane-like environment around the ferrocene with an energy contribution between FcC_6S and all the $C_{12}S$ chains of −80 kJ mol^{-1} (the same energy contribution is system A is only of −36 kJ mol^{-1}). A snapshot of the system B is shown in panel b of Figure 6.

To complete this analysis, we now focus on the molecular density profiles of water in the two films. In system A, some water molecules can approach the FcC_6S chain with an energy contribution of −45 kJ mol^{-1}. The energy contributions are calculated from the sum of the Lennard-Jones and electrostatic potentials calulated from eqs 5 and 7, respectively. In system B, the energy contribution between water and FcC_6S is only
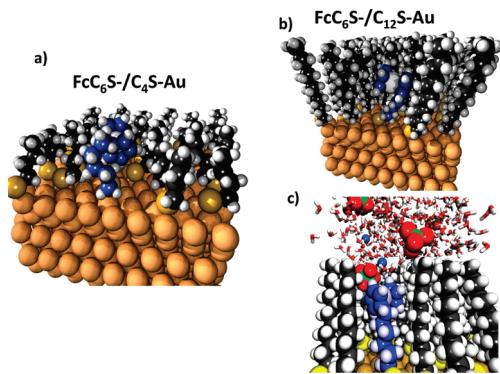
Prediction of Redox Properties of Electroactive SAMs

J. Phys. Chem. B, Vol. 114, No. 40, 2010 **12905**

Figure 6. Typical configurations of the (a) FcC_6S-/C_4S-Au system and (b) $FcC_{12}S$-/C_4S-Au SAMs at $\lambda = 0.3$. In (c), we focus on the ion-pair between the ferricynium headgroup ($\lambda = 1.0$) and the closest ClO_4^- anion.

-5.6 kJ mol^{-1}. These different distributions of water molecules induce different behaviors for the electrolyte in the two systems. In system A, a very small amount of ClO_4^- anions interact with the ferrocene moiety; we observe a small overlap between their density profiles and an energy contribution between the perchlorate anions and FcC_6S of -10 kJ mol^{-1}. In the latter one, the density profiles of FcC_6S and perchlorate anions do not overlap and we observe no energy contribution between these two species. The perchlorate anions do not enter the monolayer and prefer to be surrounded by water molecules (see Figure 5c).

As the ferrocene is oxidized ($\lambda = 1.0$), the density profiles are represented in panels b and d of Figure 5. We do not observe any significant change in the density profile of water molecules in systems A and B. In system A, the oxidation changes the density profiles of the perchlorate anions. The density profile of ClO_4^- is shifted toward the ferricinium group. This indicates that the perchlorate anions interact further with the ferricinium headgroup. Actually, the energy contribution between the perchlorate anions and FcC_6S is then -55 kJ mol^{-1} (against -10 kJ mol^{-1} in the reduced state). The binary monolayer becomes then more permeable to the perchlorate anions after oxidation. Additionally, Figure 5b shows the formation of an ion-pair between the ferricinium and one specific perchlorate anion (first peak of the ClO_4^- density profile). The energy contribution of this ion pair is about -34 kJ mol^{-1} and the average distance between the two ions is 5.9 Å. The price to be paid for this ion-pair formation is a partial dehydration of the ClO_4^- anion. Indeed, the perchlorate anion involved in the ion-pair loses three water molecules in its first hydration shell with respect to its hydration in bulk conditions. We also observe that after oxidation the density profile of the alkyl chain of FcC_6S shows peaks that are much more marked indicating that the alkyl part of the chain loses a certain mobility. This is due to stronger interactions between the ferricinium and the single perchlorate anion. As a result, the energy contribution between FcC_6S and C_4S is less favorable after oxidation, -23 versus -36 kJ mol^{-1} before oxidation.

In system B, we observe that the density profiles of the atoms of the ferricinium headgroup are shifted to a larger z suggesting a stretching of about 1 Å for the FcC_6S chain upon oxidation. As a consequence, the peaks of the density profiles of the methylene groups of FcC_6S become well separated. The energy contribution between FcC_6S and the $C_{12}S$ chains is much less favored upon oxidation (-58 against -80 kJ mol^{-1} before oxidation). We underline that the loss of energy for this

contribution ($+22$ kJ mol^{-1}) is more important in SAMs with coadsorbed $C_{12}S$ chains than in SAMs with coadsorbed C_4S chains ($+13$ kJ mol^{-1}). This energy contribution follows the same trend as the $\Delta\Delta A$ thermodynamic redox property indicating that the oxidation is more favored with shorter coadsorbed chains. However, only the total $\Delta\Delta A$ property is relevant to conclude the stability of the environment upon oxidation because it involves the sum of all the energy contributions. The perchlorate anions interact now with the FcC_6S chain with a contribution of -48 kJ mol^{-1}. Before the oxidation, this energy contribution was negligible. It means that the monolayer formed with $C_{12}S$ chains is even more permeable to perchlorate anions than that formed with C_4S chains. We also observe the formation of an ion-pair between the ferricinium and a single perchlorate anion. The energy contribution between these two ions is -48 kJ mol^{-1} with an average distance between the two center of mass of 4.8 Å. The ion-pair is stronger in system B than in system A. This result is in agreement with experiments[16] that conclude that the ion-pairing of ferricinium with perchlorate anion is more favored when the environment of the ferricinium becomes more alkane-like. However, the ion-pair formation is accompanied by a stronger desolvation of the first hydration shell of the perchlorate anion (a loss of six water molecules with respect to the bulk). This energy contribution is compensated by a favorable energy contribution between the ferricinium and ClO_4^- anion. The stretching of the FcC_6S chain is the key element to allowing the ion-pair formation and to avoiding a too important thermodynamic cost due to the desolvation of the perchlorate anion. This stretching has been already observed from recent ellipsometry[65–67] and surface plasmon resonance spectroscopy (SPR)[67,68] investigations of FcRS-Au SAMs that report a thickening of the monolayer film by 0.1–0.3 nm upon oxidation of the terminal ferrocene moieties. Panel c of Figure 6 illustrates the formation of the ion-pair between the ferricinium headgroup and a single perchlorate anion in the FcC_6S-/$C_{12}S$-Au binary SAM.

Conclusions

We have reported molecular simulations of binary monolayers containing one ferrocenylhexanethiol chain and coadsorbed n-alkanethiol chains. We have applied the thermodynamic integration method to predict the shift in the redox potential as the coadsorbed chain length increases from 4 to 12 carbons. The Helmholtz free energy has been split into different contributions to evidence the contributions of the real and reciprocal space parts of the electrostatic potential calculated with the Ewald summation technique. This theoretical aspect is very important since the calculation of free energy by molecular simulations is far from being trivial in heterogeneous systems involving changes in the electrostatic interactions.

The modeling of the binary monolayers (energy parameters and partial charges) has involved the combination of different force fields. It means that the set of parameters and charges used here is not unique and implies that the results may depend on the potential interaction models. However, we did not aim at demonstrating the transferability of a given force field but rather to show the ability of free energy perturbation methods to reproduce the change in the redox potential in electroactive SAMs when the environment of the ferrocene moiety is modified. Experiments have established a shift in redox potential of 200 mV when the coadsorbed chain changes from C_4S to $C_{12}S$ chains. It means that the oxidation of the ferrocene group is unfavored with longer coadsorbed alkylthiolate chains. The free energy calculations predict a change of about 17 versus 19

kJ mol^{-1} for experiments. To our knowledge, this is the first time that the prediction of such property in SAMs is achieved by molecular simulation. This calculation constitutes an excellent prediction and allows us to consider the free energy formalism as an efficient tools for the prediction of the redox properties of SAMs.

We have completed this work by an investigation of the initial state (reduced ferrocene) and final state (oxidized ferrocene) in the FcC$_6$S-/C$_4$S-Au and FcC$_6$S-/C$_{12}$S-Au binary SAMs. We have investigated the density profiles of the different species along the normal to the surface. The FcC$_6$S-/C$_{12}$S-Au binary SAM is shown to be more permeable to perchlorate anions than the FcC$_6$S-/C$_4$S-Au binary SAM after oxidation. We have shown the formation of an ion-pair between a single perchlorate anion and the ferricinium ion. The ion-pair is stronger in the FcC$_6$S-/C$_{12}$S-Au binary SAM. The formation of this ion-pair results from a balance between the desolvation of the perchlorate anion involved in the ion-pair and the favorable energy contribution between the two ions. The stretching of the FcC$_6$S chain contributes to reduce the thermodynamic cost due to the desolvation of the perchlorate anions and has already been observed by experiments in different SAMs.

Annihilation of the Sodium Cation

The annihilation of the sodium cation is carried out by progressively reducing the Lennard-Jones parameters and partial charge of the sodium cation to zero. Panels a and b of Figure A-1 show the average value of $\langle [\partial U(r, \lambda)]/(\partial \lambda) \rangle_\lambda$ as a function of λ along the mutation process. These curves show that the annihilation of the sodium cation leads to a linear curve for the Lennard-Jones contribution with a resulting negative ΔA value (see Table 2) for the two systems. The electrostatic contribution ΔA calculated from the real space potential is shown in panels c and d of Figure A-1 for systems A and B, respectively.
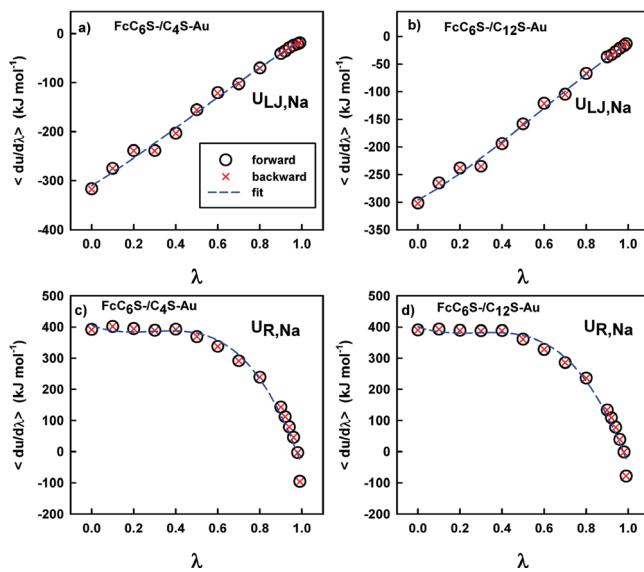

Figure A-1. Free energy derivative $\langle ((\partial U(r, \lambda))/(\partial \lambda) \rangle_\lambda$ as a function of λ for (a) and (b) the Lennard-Jones contributions and (c) and (d) the real space of the potential calculated in the FcC$_6$S-/C$_4$S-Au (panels a and c) and FcC$_6$S-/C$_{12}$S-Au (panels b and d) systems.

The dependence of $\langle [\partial U(r, \lambda)]/(\partial \lambda) \rangle_\lambda$ with λ shows a plateau between $\lambda = 0.0$ and $\lambda = 0.4$ and a deep decrease for larger λ in the two systems. The total contribution to ΔA for the annihilation of the sodium is positive. This is in line with the fact this annihilation corresponds to the opposite of the hydration process.[64]

References and Notes

(1) Chandross, M.; Grest, G. S.; Stevens, M. J. *Langmuir* **2002**, *18*, 8392.
(2) Thomas, K. G.; Kamat, P. V. *Acc. Chem. Res.* **2003**, *104*, 293.
(3) You, C. C.; De, M.; Han, G.; Rotello, V. M. *J. Am. Chem. Soc.* **2005**, *127*, 12873.
(4) Izumi, R.; Hayama, K.; Hayashi, K.; Toko, K. *Chem. Sens.* **2004**, *20*, 50.
(5) Kishimoto, M.; Ikenaga, Y.; Siigi, H.; Nagaoka, T. *Chem. Sens.* **2002**, *18*, 31.
(6) Kim, D.-S.; Park, H.-J.; Park, J.-E.; Shin, J.-K.; Kang, S.-W.; Seo, H.-I.; Lim, G. *Sens. Mater.* **2005**, *17*, 259.
(7) Campuzano, S.; Pedrero, M.; Pingarron, J. *Talanta* **2005**, *66*, 1310.
(8) Kitagawa, K.; Morita, T.; Kimura, S. *Langmuir* **2005**, *21*, 10624.
(9) Chen, J.; Reed, M. A.; Rawlett, A. M.; Tour, J. M. *Science* **1999**, *286*, 1550.
(10) Andres, R. P.; Bein, T.; Dorogi, M.; Feng, S.; Henderson, J. I.; Kubiak, C. P.; Mahoney, W.; Osifchin, R. G.; Reifenberger, R. *Science* **1996**, *272*, 1323.
(11) Chidsey, C. E. D.; Bertozzi, C. R.; Putwinski, T. M.; Mujsce, A. M. *J. Am. Chem. Soc.* **1990**, *112*, 4301.
(12) Chidsey, C. E. D. *Science* **1991**, *251*, 919.
(13) Smalley, J. F.; Feldberg, S. W.; Chidsey, C. E. D.; Linford, M. R.; Newton, M. D.; Liu, Y.-P. *J. Phys. Chem.* **1995**, *99*, 13141.
(14) Creager, S. E.; Rowe, G. K. *Anal. Chim. Acta* **1991**, *246*, 233.
(15) Creager, S. E.; Rowe, G. K. *J. Electroanal. Chem.* **1994**, *370*, 203.
(16) Rowe, G. K.; Creager, S. E. *Langmuir* **1991**, *7*, 2307.
(17) Weber, K.; Hockett, L.; Creager, S. *J. Phys. Chem. B* **1997**, *101*, 8286.
(18) Sumner, J. J.; Weber, K. S.; Hockett, L. A.; Creager, S. E. *J. Phys. Chem. B* **2000**, *104*, 7449.
(19) Collard, D. M.; Fox, M. A. *Langmuir* **1991**, *7*, 1192.
(20) Buttry, D. *Langmuir* **1990**, *6*, 1319.
(21) Lee, L. Y. S.; Sutherland, T. C.; Rucareanu, S.; Lennox, R. B. *Langmuir* **2006**, *22*, 4438.
(22) Goujon, F.; Bonal, C.; Malfreyt, P. *Mol. Sim.* **2009**, *35*, 538–546.
(23) Goujon, F.; Bonal, C.; Limoges, B.; Malfreyt, P. *Langmuir* **2009**, *25*, 9164.
(24) Goujon, F.; Bonal, C.; Limoges, B.; Malfreyt, P. *J. Phys. Chem. B* **2008**, *112*, 14221.
(25) Goujon, F.; Bonal, C.; Limoges, B.; Malfreyt, P. *J. Phys. Chem. B* **2010**, *114*, 6447.
(26) Zwanzig, R. W. *J. Chem. Phys.* **1954**, *22*, 1420.
(27) Mezei, M.; Swaminathan, S.; Beveridge, D. L. *J. Am. Chem. Soc.* **1978**, *100*, 3255.
(28) Mezei, M.; Beveridge, D. L. *Ann. N.Y. Acad. Sci.* **1986**, *482*, 1.
(29) Pearlman, D. A. *J. Comput. Chem.* **1994**, *105*, 105.
(30) Ghoufi, A.; Bonal, C.; Morel, J. P.; Morel-Desrosiers, N.; Malfreyt, P. *J. Phys. Chem. B* **2004**, *108*, 11744.
(31) Ghoufi, A.; Malfreyt, P. *Mol. Phys.* **2006**, *104*, 2929.
(32) Swope, W. C.; Andersen, H. C. *J. Phys. Chem.* **1984**, *88*, 6548.
(33) Jörgensen, W. L. *Encyclopedia of Computational Chemistry*; Schleyer, P., Ed.; Wiley: New-York, 1998; Vol. 2.
(34) Lamb, M. L.; Jörgensen, W. L. *Curr. Opini. Chem. Biol.* **1997**, *1*, 449.
(35) Jörgensen, W. L.; Duffy, E. M.; Essex, J. W.; Severance, D. L.; Blake, J. F. *Biomolecular Structure and Dynamics*; Vergoten, G., Theophanides, T., Eds.; Kluwer: Amsterdam, The Netherlands, 1997.
(36) Bohm, H. J.; Klebe, G. *Angew. Chem., Int. Ed. Engl.* **1996**, *35*, 2588.
(37) Buckner, J. K.; Jörgensen, W. L. *J. Am. Chem. Soc.* **1989**, *111*, 2507.
(38) Rao, B. G.; Singh, U. C. *J. Am. Chem. Soc.* **1989**, *111*, 3125.
(39) Rizzo, R. C.; Jörgensen, W. L. *J. Am. Chem. Soc.* **1999**, *121*, 4827.
(40) Sattelle, B. M.; Sutcliffe, M. J. *J. Phys. Chem. A* **2008**, *112*, 13053.
(41) Roy, L. E.; Jakubikova, E.; Guthrie, M. G.; Batista, E. *J. Phys. Chem. A* **2009**, *113*, 6754.
(42) Li, J.; Fisher, C. L.; Chen, J. L.; Basheford, D.; Noodleman, L. *Inorg. Chem.* **1996**, *35*, 4694.
(43) Tavernelli, I.; Vuillemier, R.; Sprik, M. *Phys. Rev. Lett.* **2002**, *88*, 213002.
(44) Min, D.; Zheng, L.; Harris, W.; Chen, M.; Lv, C.; Yang, W. *J. Chem. Theory Comput.* **2010**, *6*, 2253.

Prediction of Redox Properties of Electroactive SAMs

J. Phys. Chem. B, Vol. 114, No. 40, 2010 **12907**

(45) Cornell, W. D.; Cieplak, P.; Bayly, C. I.; Gould, I. R.; Merz, K. J.; Ferguson, D. M.; Spellmeyer, D. M.; Fox, T.; Caldwell, J. W.; Kollman, P. *J. Am. Chem. Soc.* **1995**, *117*, 5179.

(46) Rai, B.; Sathish, P.; Malhotra, C. P.; Pradip; Ayappa, K. G. *Langmuir* **2004**, *20*, 3138.

(47) Lopes, J. N. C.; do Couto, P. C.; da Piedade, M. E. M. *J. Phys. Chem. A* **2006**, *110*, 13850.

(48) Ryckaert, J. P.; Cicotti, G.; Berendsen, H. J. C. *J. Comput. Phys.* **1977**, *23*, 327.

(49) Abascal, J. L. F.; Vega, C. *J. Chem. Phys.* **2005**, *123*, 234505.

(50) Goujon, F.; Bonal, C.; Limoges, B.; Malfreyt, P. *Mol. Phys.* **2008**, *106*, 1397.

(51) Klähn, M.; Seduraman, A.; Wu, P. *J. Phys. Chem. B* **2008**, *112*, 10989.

(52) Allen, M. P.; Tildesley, D. J. *Computer Simulation of Liquids*; Oxford University Press: Clarendon, 1981.

(53) Smith, E. R. *Proc. R. Soc. London, Ser. A* **1981**, *375*, 475.

(54) Yeh, I.-C.; Berkowitz, M. L. *J. Chem. Phys.* **1999**, *111*, 3155.

(55) Hoover, W. G. *Phys. Rev. A* **1985**, *31*, 1695.

(56) DL_POLY is a parallel molecular dynamics simulation package developed at the Daresbury Laboratory Project for Computer Simulations under the auspices of the EPSRC for the Collaborative Computational Project for Computer Simulation of Condensed Phases (CCP5)) is a parallel molecular dynamics simulation package developed at the Daresbury Laboratory Project for Computer Simulations under the auspices of the EPSRC for the Collaborative Computational Project for Computer Simula- tion of Condensed Phases (CCP5) and the Advanced Research Computing Group (ARCG) at the Daresbury Laboratory.

(57) Honenberg, P.; Kohn, W. *Phys. Rev. A* **1964**, *136*, 864.

(58) Kohn, W.; Sham, L. *J. Phys. Rev. A* **1965**, *140*, 1133.

(59) Becke, A. D. *Phys. Rev. A* **1988**, *38*, 3098.

(60) Becke, A. D. *J. Chem. Phys.* **1993**, *98*, 5648.

(61) Perdew, J. P.; Wang, Y. *Phys. Rev. E* **1991**, *45*, 13244.

(62) Frisch, M. J.; Trucks, G. W.; Schelgel, H. B.; Scuseria, G. E.; Robb, M. A.; Cheesemann, J. R.; Montgomery, J. A.; Kudin, K. N.; Burant, J. C.; Millam, J. M.; Iyengar, S. S.; Tomasi, J.; Barone, V.; Mennucci, B.; Cossi, M.; Scalmani, G.; Rega, N.; Petersson, G. A.; Nakajima, T.; Honda, Y.; Kitao, O.; Nakai, H.; Klene, M.; Li, X.; Knox, J. E.; Hratchian, H. P.; Cross, J. B.; Bakken, V.; Adamo, C.; Jaramillo, J.; Gomperts, R.; Stratmann, R. E.; Yazyev, O.; Austin, A. J.; Cammi, R.; Pomelli, C.; Ochterski, J. W.; Ayala, P. Y.; Morokuma, K.; Voth, G. A.; Salvador, P.; Dannenberg, J. J.; Zakrzewski, V. G.; Dapprich, S.; Daniels, A. D.; Strain, M. C.; Farkas, O.; Malick, D. K.; D.Rabuck, A.; Raghavachari, K.; Foresman, J. B.; Ortiz, J. V.; Cui, Q.; Baboul, A. G.; Clifford, S.; Ciolkowski, J.; Stefanov, B. B.; Liu, G.; Liashenko, A.; Piskorz, P.; Komaromi, I.; Martin, R. L.; Fox, D. J.; Keith, T.; Al-Laham, M. A.; Peng, C. Y.; Nanayakkara, A.; Challacombe, M.; Gill, P. M. W.; Johnson, B.; Chen, W.; Wong, M. W.; Gonzalez, C.; Pople, J. A. *Gaussian 03*, revision D.01; Gaussian, Inc.: Wallingford, CT, 2004.

(63) Breneman, C. P.; Wiberg, K. B. *J. Comput. Chem.* **1990**, *11*, 361.

(64) Marcus, Y. *Liquid−Liquid Interfaces Theory and methods*; CRC Press: Boca Raton, FL, 1996.

(65) Viana, A. S.; Jones, A. H.; Abrantes, L.; Kalaji, M. *J. Electroanal. Chem.* **2001**, *500*, 290.

(66) Abrantes, L. M.; Kalaji, M.; Viana, A. S. *Russ. J. Electrochem.* **2002**, *38*, 39.

(67) Yao, X.; Wang, J.; Zhou, F.; Wang, J.; Tao, N. *J. Phys. Chem. B* **2004**, *108*, 7206.

(68) Norman, L.; Badia, A. *Langmuir* **2007**, *23*, 10198.